ACS Catalysis

Research Article

pubs.acs.org/acscatalysis

Promoting Effect of Sulfur Addition on the Catalytic Performance of Ni/$MgAl_2O_4$ Catalysts for Isobutane Dehydrogenation

Guowei Wang, Zhe Meng, Jianwei Liu, Chunyi Li,* and Honghong Shan

State Key Laboratory of Heavy Oil Processing, China University of Petroleum, Qingdao 266580, PR China

Supporting Information

ABSTRACT: Ni/$MgAl_2O_4$ catalysts with high NiO loadings were highly active for isobutane cracking, which led to abundant formation of methane, hydrogen and coke. The results of activity testing and XRD characterization jointly revealed that large ensembles of metallic nickel species formed during reaction notably catalyzed cracking instead of dehydrogenation. However, after introduction of sulfur into Ni/$MgAl_2O_4$ catalyst through impregnation with ammonium sulfate, undesired cracking reactions were effectively inhibited, and the selectivity to isobutene increased remarkably. Totally, up to ~42 wt % isobutene could be obtained at 560 °C in a single pass after the modification. From the characterization results, it was also concluded that, after sulfur introduction, NiO particles became much smaller and better dispersed on the catalyst surface. NiS species, formed during the induction period of the reaction, not only facilitated isobutene desorption from the catalyst, but also constituted the active sites for isobutane dehydrogenation. In addition, due to the appearance of NiS species, Ni/$MgAl_2O_4$ catalyst after H_2S/H_2 sulfuration exhibited a high initial activity without experiencing an induction period, further confirming the crucial role that introduced sulfur played.

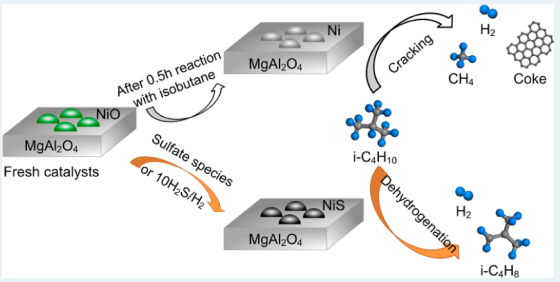

KEYWORDS: *isobutane, dehydrogenation, Ni/$MgAl_2O_4$ catalysts, sulfur addition, NiS*

1. INTRODUCTION

Driven largely by the increasing demand for isobutene, which has been widely applied in the production of polyisobutene (PIB), methyl tertiary butyl ether (MTBE), and methyl methacrylate (MMA), the technologies for isobutane dehydrogenation have attracted much attention in recent years.

Two kinds of catalysts commercially applied for catalytic dehydrogenation of isobutane are chromia-based[1−3] and platinum-based catalysts.[4−6] Although relatively satisfactory performance has been achieved, both of them possess their own disadvantages. Cr^{6+} species are harmful to humans and the environment during both preparation and application processes, while for Pt-based catalysts, high investment and operating costs are inevitable. Up to now, the development of a novel catalyst system with relatively inexpensive and environmentally friendly characteristics is still one of the urgent issues.

Nickel oxide, known to be active in many important reactions for decades, such as water−gas shift[7−9] and steam reforming of methane[10,11] and ethanol,[12,13] may be an attractive alternative. Some researchers[14−20] have investigated the reaction mechanism of gas phase transition metal ions with light alkanes to determine the factors governing C−C and C−H bond cleavage ratios. Georgiadis et al.[14] and Jacobson et al.[20] reported that nickel ions were prone to insert into the weakest C−C bond rather than the C−H bond; consequently, cracking reactions occurred. Although these homogeneous catalytic reactions investigated in the gas phase have little practical value, the theories developed provide profound guidance to deepen the understanding of the nature of dehydrogenation.

In 1994, Resasco and his co-workers[21] found that nickel-based catalysts exhibited high catalytic activity but low selectivity toward olefins in isobutane dehydrogenation, and as a result of the rapid cracking reactions, abundant methane and coke were generated. Since the breakage of C−C bond occurs preferentially under the catalysis of nickel species, greater efforts should be made to selectively activate alkanes to achieve higher selectivities toward olefins in alkane dehydrogenation.[22] To activate the alkanes selectively, two important aspects should not be overlooked: (1) to inhibit C−C bond rupture[23] to reduce the possibility of cracking reactions and (2) to facilitate desorption of the olefin produced[24,25] to avoid undesired secondary reactions. To achieve the above objectives, the researchers[21] introduced a certain amount of dimethyl sulfoxide into Ni/Al_2O_3 catalyst and found that the selectivity to isobutene was improved effectively, but both the activity and stability still needed to be improved. Moreover, the liquids containing sulfur are generally hazardous and malodorous. Therefore, in this study, relatively safe sulfate species are introduced to modify the nickel-based catalysts instead.

In this study, Ni/$MgAl_2O_4$ catalysts with different NiO loadings were prepared and evaluated for catalytic dehydrogen-

Received: August 20, 2013
Revised: November 10, 2013
Published: November 11, 2013

   dx.doi.org/10.1021/cs400705p | ACS Catal. 2013, 3, 2992−3001

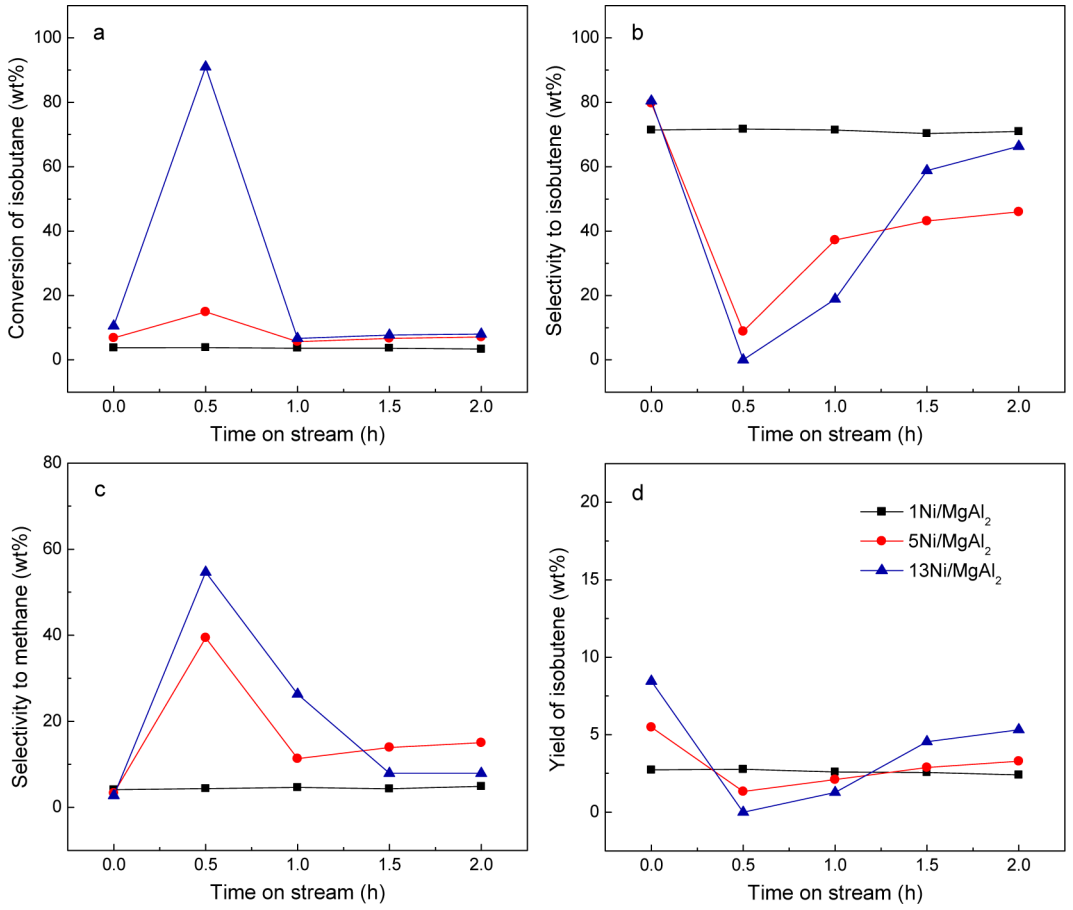

Figure 1. Dehydrogenation performance of Ni/$MgAl_2O_4$ catalysts with different NiO loadings.

ation of isobutane. Moreover, sulfur modified Ni/$MgAl_2O_4$ catalysts were prepared by impregnation of ammonium sulfate and catalytic performance was also evaluated. Experimental results demonstrated that improved dehydrogenation performance was achieved for the sulfur modified catalysts. Subsequently, the effects of sulfur addition on surface structure, redox properties and adsorption−desorption behaviors of Ni/$MgAl_2O_4$ catalyst were investigated, and the active species for dehydrogenation were also speculated. Furthermore, sulfuration of Ni/$MgAl_2O_4$ catalyst with H_2S/H_2 was carried out to gain deeper insight into the nature of the active phase.

2. EXPERIMENTAL SECTION

2.1. Catalyst Preparation. $MgAl_2O_4$ was prepared by the sol−gel method. Pseudoboehmite powder was mixed with distilled water in a vessel to obtain a suspended solution, and then HCl solution was added dropwise under vigorous stirring at 70 °C. After that, an appropriate amount of magnesium nitrate solution was added. The gel was stirred for 4 h, dried at 140 °C overnight, and calcined at 700 °C in air for 4 h. Finally, the support was crushed and sieved to 80−180 μm for later use.

Nickel oxide catalysts supported on $MgAl_2O_4$ were prepared by incipient wetness impregnation with appropriate amounts of nickel nitrate. Sulfur modified Ni/$MgAl_2O_4$ catalysts were obtained by sequential impregnation of $MgAl_2O_4$ with aqueous ammonium sulfate and nickel nitrate solutions. After impregnation, the catalysts were dried at 140 °C overnight and calcined at 700 °C in air for 2 h. The as-prepared catalysts are denoted as xNi/$MgAl_2$ for the unmodified catalysts and xNi/$MgAl_2$−S for the catalysts with sulfur addition, respectively, where x represents the content of nickel oxide by weight, and the content of SO_4^{2-} was 5 wt % for the sulfur-modified catalysts.

2.2. Catalyst Characterization. Specific surface areas and pore structure properties of the catalysts were determined by adsorption−desorption measurements of nitrogen at liquid nitrogen temperature using a Quadrasorb SI instrument. Prior to the measurement, all samples were evacuated at 300 °C for 4 h at a pressure of 1.0×10^{-3} kPa to ensure complete removal of adsorbed moisture. X-ray diffraction (XRD) of the catalysts was carried out on an X'Pert PRO MPD diffractometer system using Cu Kα radiation at 40 kV and 40 mA, running from 5° to 75° with a speed of 10°/min. And SEM images were obtained using HITACHI S-4800 scanning electronic microscope.

The redox behavior of catalyst samples was determined by temperature-programmed reduction of hydrogen (H_2-TPR). During the test, about 0.1 g of sample was loaded into the apparatus, preheated in a flow of helium at 200 °C for 0.5 h, and then cooled down to 80 °C. Subsequently, the sample was brought into contact with a mixture of 10 vol. % H_2/N_2 (30 mL/min) and heated at a rate of 10 °C/min to the final temperature. The effluent gas passed through a thermal conductivity detector and was analyzed with a GAS-100Q mass spectrometer.

To investigate the adsorption and desorption behaviors of the catalysts for alkanes and alkenes, isobutane and isobutene adsorption−desorption tests were performed with a FINESORB-3010 chemisorption analyzer, and the gas released from

dx.doi.org/10.1021/cs400705p | ACS Catal. 2013, 3, 2992−3001

the reactor was analyzed by an online GAS-100Q quadrupole mass spectrometer. A schematic of the apparatus is shown in Figure S1 in the Supporting Information. For each test, about 0.2 g of catalyst was loaded into a quartz tube reactor, preheated in a flow of nitrogen (60 mL/min) at 450 °C for 0.5 h, and then cooled to 50 °C. Subsequently, the nitrogen flow was instantaneously switched to a mixture of Ar (30 mL/min) and isobutane or isobutene (30 mL/min). Compared with the insert gas, detection of hydrocarbon was delayed to some extent due to adsorption on the catalyst surface, and a large difference between the signals of inert gas and hydrocarbon implied a stronger adsorption ability of the catalysts for isobutane or isobutene. For the tests of hydrocarbon desorption, the flow was switched back to nitrogen after adsorption saturation.

2.3. Catalytic Activity Test. Isobutane dehydrogenation was conducted using a fixed bed microreactor at 560 °C under atmospheric pressure with 4 g of catalysts (80−180 μm) loaded into the reactor. Prior to reaction, catalysts were degassed at reaction temperature in a nitrogen flow to remove adsorbed oxygen and water from the catalyst surface. During the test, isobutane was fed to the reactor at a fixed flow rate of 2 mL/min with a nitrogen flow of 12 mL/min. The composition of effluent gaseous products was analyzed by a Bruker 450 Gas Chromatograph equipped with a FID detector to determine the composition of hydrocarbons and two TCD detectors to analyze the content of hydrogen, carbon monoxide, and carbon dioxide. Through analyzing the quantity of CO_2 generated during in situ coke combustion with the chromatogram, the amount of coke deposited on the catalysts after reaction was determined.

Isobutane conversion and product selectivity are calculated as follows:

$$\text{isobutane conversion} = \frac{\text{isobutane, in} - \text{isobutane, out}}{\text{isobutane, in}} \times 100\ \text{wt\%} \quad (1)$$

$$\text{selectivity to product } i = \frac{i\text{, out}}{\text{isobutane, in} - \text{isobutane, out}} \times 100\ \text{wt\%} \quad (2)$$

3. RESULTS AND DISCUSSION

3.1. Dehydrogenation Performance of $Ni/MgAl_2O_4$ Catalysts. Isobutane dehydrogenation over $Ni/MgAl_2O_4$ catalysts with different NiO loadings was evaluated in the fixed bed microreactor at 560 °C, and the results are displayed in Figure 1. It is apparent that the dehydrogenation performance is strongly affected by NiO loading. As for $1Ni/MgAl_2$ catalyst, a very low and steady activity lasting for 2 h was observed, while the selectivity to isobutene was maintained at a high level. With increasing NiO loading, the catalytic performance changed significantly. As the reaction proceeded, the isobutane conversion first increased and then decreased dramatically for both $5Ni/MgAl_2$ and $13Ni/MgAl_2$ catalysts; meanwhile, the selectivity to isobutene exhibited the opposite trend with time on stream (TOS). It is also worth noting that, with decreasing selectivity toward isobutene, abundant methane was generated, indicating the transformation from dehydrogenation to undesirable cracking reactions. In general, due to the low isobutane conversion at low NiO loadings and inferior selectivity to isobutene at high loadings, isobutene yield was unsatisfactory for the investigated catalysts.

Possibly resulting from structural changes in surface nickel species during reaction, the desired dehydrogenation reaction was transformed to cracking reactions, most probably hydrogenolysis reactions with the presence of hydrogen produced in the dehydrogenation reaction, and consequently, abundant methane was generated at reaction time 0.5 h. After 2 h reaction, the coke contents of $Ni/MgAl_2O_4$ catalysts with NiO loadings of 1, 5, and 13 wt % were 0.09, 1.93, and 3.55 wt %, respectively. Therefore, the decreasing isobutane conversion with TOS could mainly be attributed to the coverage of active sites by coke deposition. And consistent with the variation trend of coke yield, the deactivation rate also increased with NiO loading.

To further investigate the possible transformation of nickel phase during the reaction, XRD characterization of both the fresh $13Ni/MgAl_2$ catalyst and the catalyst reacted for 0.5 h, the latter of which exhibited highest cracking activity and yielded most methane, was carried out. In the XRD patterns displayed in Figure 2, NiO, $MgAl_2O_4$, and $NiAl_2O_4$ (the latter two presented indistinguishable characteristic peaks) were all detected on the fresh catalyst. With regard to $13Ni/MgAl_2$ catalyst reacted for 0.5 h, the intensity of diffraction peaks for NiO decreased, and additional peaks characteristic of metallic nickel were observed. It has been reported that metallic nickel is extremely active for C−C bond scission;[26] moreover, it is also believed that the hydrogenolysis of alkanes occurs rapidly under the catalysis of Ni-based catalysts,[21] which leads to abundant formation of methane, coke and hydrogen. Therefore, it could be concluded that the metallic nickel species generated during

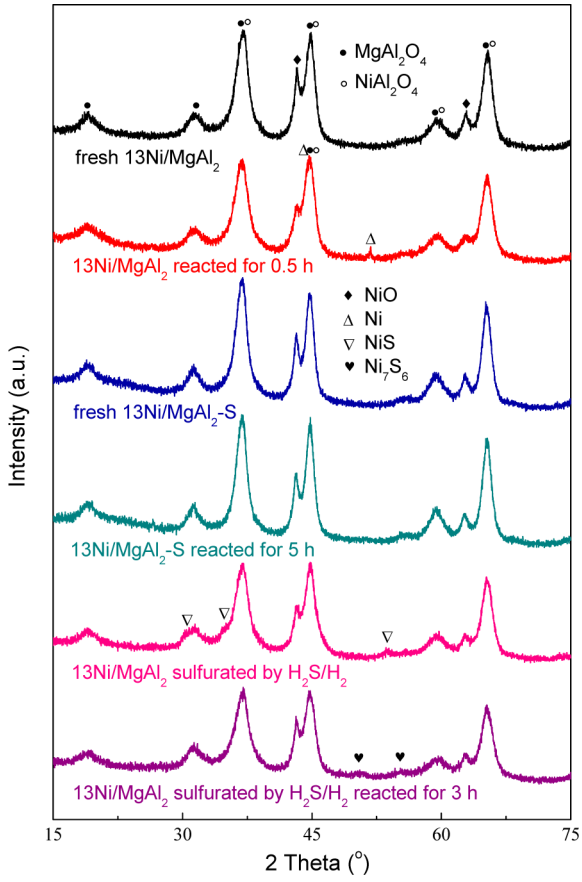

Figure 2. XRD patterns of different $13Ni/MgAl_2$ catalysts.

dx.doi.org/10.1021/cs400705p | ACS Catal. 2013, 3, 2992−3001

the reaction facilitated the undesired cracking reactions, and at the same time, the dehydrogenation reaction was weakened. One possible explanation for the low cracking activity of the catalysts with low NiO loading is that the hydrogenolysis reaction is structure sensitive and a large ensemble of nickel atoms are required to constitute the active sites and catalyze the reaction.[21] Furthermore, to detect the nickel ensembles directly, SEM images of both 1Ni/$MgAl_2$ and 13Ni/$MgAl_2$ catalysts after 0.5 h of reaction have been taken, as shown in Figure S2 in the Supporting Information. As for 1Ni/$MgAl_2$ catalyst, the nickel species on the support were highly dispersed and hardly aggregated together. In contrast, the surface of 13Ni/$MgAl_2$ catalyst was covered by plentiful nickel species, and nickel ensembles with average diameters of about 1.5 μm were also observed, which were likely responsible for hydrogenolysis. Moreover, the reduction process becomes much more difficult for smaller NiO particles,[27] which also restricted the undesired reactions.

In general, Ni/$MgAl_2O_4$ catalysts with low NiO loadings exhibited poor activity, while undesired cracking reactions, most probably hydrogenolysis reactions catalyzed by the aggregated metallic nickel formed during the reaction, occurred at high loadings. Consequently, further work is still required to improve the catalytic performance.

3.2. Effect of Sulfur Introduction into Ni/$MgAl_2O_4$ Catalysts. *3.2.1. Dehydrogenation Performance and Reaction Kinetics.* To improve the dehydrogenation performance of the catalysts, many attempts have been carried out. Among them, sulfur modification by impregnating the catalyst with ammonium sulfate improved the catalyst performance impressively, which was in accordance with the excellent activation ability that the sulfide catalysts behaved in the hydrogenation reaction,[28−30] that is, reverse reaction to dehydrogenation. Activity test results of the 13Ni/$MgAl_2$−S catalyst are displayed in Figure 3, and detailed comparison with the properties and performance of 13Ni/$MgAl_2$ catalyst without sulfur addition is shown in Table 1.

Compared with the catalyst with no sulfur addition, the initial isobutane conversion over 13Ni/$MgAl_2$−S catalyst exhibited little difference, while the initial selectivity to isobutene was much lower due to the formation of a large amount of CO_x (not shown). Moreover, both the isobutane conversion and selectivity toward isobutene increased gradually

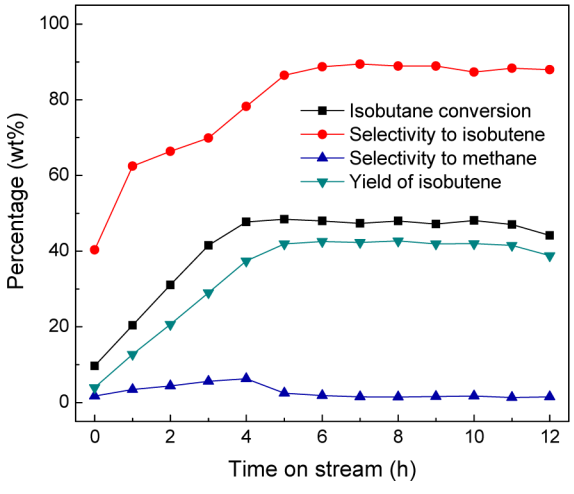

Figure 3. Dehydrogenation performance of 13Ni/$MgAl_2$−S catalyst.

Table 1. Properties and Reaction Results of 13Ni/$MgAl_2$ Catalysts Before and After Sulfur Addition

item		13Ni/$MgAl_2$[e]	13Ni/$MgAl_2$[f]	13Ni/$MgAl_2$−S[e]	13Ni/$MgAl_2$−S[g]
S_{BET}[a] (m^2/g)		80		84	
D_p[b] (nm)		7.9		6.5	
R[c] (mmol h^{-1} g^{-1})				0.6	
selectivity[d] (wt%)	methane	54.6	56.2	2.6	9.3
	ethane	0	0	0.2	4.0
	ethene	0	0	0.2	3.9
	propane	0	0	0.3	3.0
	propene	0	0	1.5	10.5
	n-butane	0	0.1	0.1	2.5
	n-butene	0	1.8	1.4	3.2
	i-butene	0	8.4	86.5	52.6
	H_2	3.1	3.3	3.9	5.4
	CO_2	0.2	0.6	0	0
	CO	2.2	2.6	2.7	1.7
	coke	39.9	26.8	0	1.4
	other product	0	0.2	0.6	2.5
conversion[d] (wt%)		91.0	48.9	48.4	90.7

[a]Specific surface area. [b]Pore size. [c]Formation rate of isobutene per mass of catalyst. [d]Data were collected after 0.5 h reaction for 13Ni/$MgAl_2$ catalyst and after 5 h reaction for 13Ni/$MgAl_2$−S catalyst, when maximum isobutane conversion was achieved. And product selectivity data have been normalized. [e]Catalytic performances of 13Ni/$MgAl_2$ and 13Ni/$MgAl_2$−S catalysts obtained at the same reaction conditions as described in the Experimental Section. [f]Catalytic performance of 13Ni/$MgAl_2$ catalyst obtained at similar conversion level with 13Ni/$MgAl_2$−S catalyst under different reaction conditions. [g]Catalytic performance of 13Ni/$MgAl_2$−S catalyst obtained at similar conversion level with 13Ni/$MgAl_2$ catalyst under different reaction conditions.

with TOS in the first 5 h of the reaction, suggesting the existence of an induction period for 13Ni/$MgAl_2$−S catalyst. Similar induction periods have also been reported for Mo-based catalysts[31] and In-based catalysts,[32−34] which were considered to be the result of the variation of valence state or structure of surface species. Moreover, the selectivity to methane was constantly kept at a very low level during the continuous 12 h reaction, which indicated that the cracking reactions were effectively inhibited by the sulfur modification. At the steady stage of the reaction for sulfur modified catalyst, lasting from 6 to 10 h, isobutene selectivity up to 90 wt % and isobutene yield higher than 40 wt % were both obtained. And after that, slightly decreasing isobutane conversion due to catalyst deactivation was observed.

For 13Ni/$MgAl_2$ catalysts before and after sulfur introduction, the reaction conditions were adjusted to obtain the product distributions at similar conversion levels. As listed in Table 1, at similar conversion levels, the isobutene selectivity increased significantly after sulfur introduction to the catalyst; simultaneously, the selectivity to methane decreased remarkably. It should be mentioned here that the reaction temperature was elevated significantly to obtain the high isobutane conversion over 13Ni/$MgAl_2$−S catalyst; therefore, the undesired thermal cracking reactions inevitably occurred, leading to decreased selectivity to isobutene.

To investigate possible phase transformation of the catalysts with TOS, 13Ni/$MgAl_2$−S catalysts before and after reaction were both characterized. XRD patterns (see Figure 2) of the fresh 13Ni/$MgAl_2$−S catalyst were similar with the catalyst

dx.doi.org/10.1021/cs400705p | ACS Catal. 2013, 3, 2992−3001

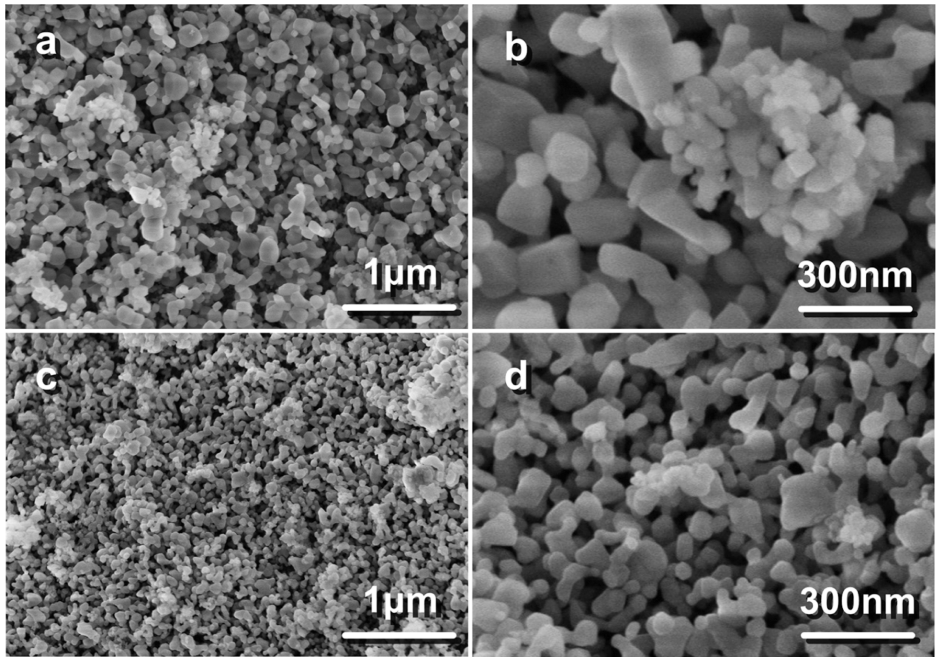

Figure 4. SEM images of 13Ni/$MgAl_2$ catalysts before and after sulfur addition: (a, b) 13Ni/$MgAl_2$ and (c, d) 13Ni/$MgAl_2$−S.

without sulfur addition due to the low SO_4^{2-} content of 5 wt %. As for the 13Ni/$MgAl_2$−S catalyst after 5 h reaction, no diffraction peak corresponding to metallic nickel was detected, suggesting that the nickel oxide on the catalyst surface was possibly not yet reduced during the continuous 5 h reaction, or the metallic nickel species formed were likely to be well dispersed on the catalyst surface. Consequently, the rapid cracking reactions activated by large ensembles of metallic nickel were inhibited remarkably. Moreover, after the introduction of sulfur, the coke content of the used catalyst decreased dramatically, from 3.55 wt % to less than 0.01 wt %, which was consistent with the reported results of Resasco et al.[21] that the pretreatment of nickel-based catalysts with dimethyl sulfoxide significantly inhibited the coke formation in isobutane dehydrogenation. As such, a low coke formation rate over the catalyst with sulfur addition guaranteed a relatively stable catalytic activity after the induction period.

To further study the reaction kinetics, isobutane dehydrogenation over 13Ni/$MgAl_2$−S catalyst was carried out in a fixed bed reactor at different temperatures ranging from 540 to 600 °C with various isobutane flow rates under atmospheric pressure, and all experimental data were collected at the steady state rather than the induction period of the reaction. According to the open literature,[35,36] a power law model neglecting adsorption of isobutane and isobutene was adopted for the dehydrogenation kinetics as follows, where r represents reaction rate, k_1 and K_{eq} stand for reaction rate constant of isobutane dehydrogenation and equilibrium constant, respectively.

$$-r_{C_4H_{10}} = k_1\left(P_{C_4H_{10}} - \frac{P_{C_4H_8}P_{H_2}}{K_{eq}}\right) \quad (3)$$

Accordingly, the value of the frequency factor for isobutane dehydrogenation in this work was estimated to be 9.2×10^6, and an activation energy of 84 kJ/mol was also obtained, which was much lower than that of 133−142 kJ/mol for isobutane dehydrogenation over Cr_2O_3/Al_2O_3 catalyst[37] and 95 kJ/mol over Pt/Sn/SiO_2 catalyst.[38]

3.2.2. Structure Characteristics of the Catalysts. To investigate the interaction of introduced sulfur with the support and nickel species after calcination, 13Ni/$MgAl_2$−S catalyst with SO_4^{2-} content of 15 wt % was prepared and characterized by XRD, with the patterns illustrated in Figure S3 in the Supporting Information. In addition to peaks characteristic of $MgAl_2O_4$, $NiAl_2O_4$ and NiO, additional peaks characteristic of $MgSO_4$ were also detected, indicating that the sulfate introduced was interacting preferentially with MgO in the support.

SEM images shown in Figure 4 illustrate the differences in the morphology of surface species on 13Ni/$MgAl_2$ catalysts before and after sulfur introduction. For the catalyst without sulfur addition (see Figure 4a, b), the catalyst surface was densely covered by a large amount of uniformly distributed cubic crystals (100−200 nm in length). Given the morphology of 1Ni/$MgAl_2$ catalyst (see Figure S2a in the Supporting Information) in which the support $MgAl_2O_4$ was basically exposed, these semicubic particles were speculated to be NiO. Meanwhile, a certain amount of aggregated NiO particles were also observed. In contrast, after the introduction of sulfur, relatively long cubic NiO crystals were transformed to small crystals (20−80 nm in length) (see Figure 4c,d).

This observation is consistent with the increase in specific surface area and the decrease in pore size (as listed in Table 1). The large ensembles of VIII metal were reported to be active for cracking reactions.[39,40] It has been reported that,[41] with the combined effect of rhenium and sulfur, the surface platinum on the catalyst was divided into tiny particles, and then a highly selective catalyst with mild dehydrogenation activity and good stability was obtained. In this work, the introduction of sulfur also seemed to prevent the nickel species from aggregating, and thus inhibiting the formation of agglomerated metallic nickel species and undesired cracking reactions, consistent with the results of XRD characterization and activity tests.

dx.doi.org/10.1021/cs400705p | *ACS Catal.* 2013, 3, 2992−3001

3.2.3. Redox Behaviors of the Catalysts. As evidenced by the experimental results, metallic nickel and nickel oxide species on the catalyst surface exhibited different catalytic behaviors; therefore, the dehydrogenation performance of the catalysts is directly related to their reduction properties. Accordingly, H_2-TPR was carried out to investigate the effect of sulfur addition on the redox behaviors of $Ni/MgAl_2O_4$ catalysts, and the H_2-TPR profiles are shown in Figure 5.

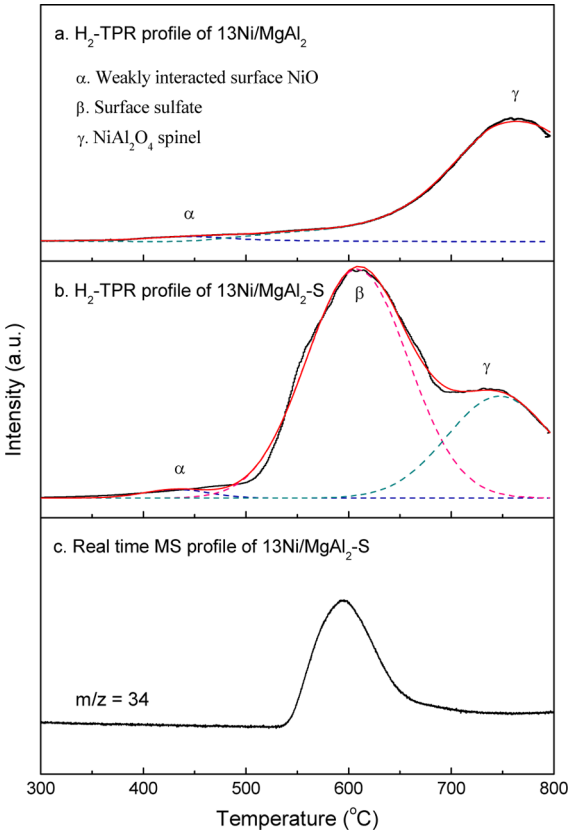

Figure 5. H_2-TPR and real time MS profiles of different $13Ni/MgAl_2$ catalysts.

As for the fresh $13Ni/MgAl_2$ catalyst (as displayed in Figure 5a), the appearance of a weak reduction peak extending from 350 to 500 °C was speculated to be caused by the reduction of nickel oxide species weakly interacting with the support to metallic nickel species. In addition, a major peak around 760 °C was also observed, which was reported to result from the reduction of other nickel species closely interacting with the support - for instance, in the form of $NiAl_2O_4$.[42−44]

For the H_2-TPR profile of $13Ni/MgAl_2$−S catalyst, three reduction peaks appeared (as displayed in Figure 5b). Compared with $13Ni/MgAl_2$ catalyst, the intensity of the low temperature peak increased to some extent, indicating that, apart from the reduction of dispersed NiO species, partial reduction of introduced sulfate species might also occur. Moreover, a newly emerged large reduction peak around 600 °C was observed. To determine the origin of this peak, an online MS spectrometer has been applied to detect the released gases during the TPR process. As illustrated in Figure 5c, a peak around 600 °C in the MS spectra corresponding to the formation of H_2S was detected, indicating that the newly emerged peak was attributed to the reduction of sulfate species introduced. And it was also worth noting that the sulfate species could even be reduced at a reaction temperature of 560 °C, which made possible the formation of metal sulfides. Moreover, as for the high temperature reduction peak in Figure 5a and Figure 5b, no obvious variation was observed.

3.2.4. Adsorption and Desorption Behaviors for Isobutane and Isobutene. Adsorption and desorption are important steps in heterogeneous catalytic reactions, and generate significant impacts on the catalytic behaviors of the catalysts. Strong adsorption of the reactants increases the possibility of the reaction and thus facilitates the conversion of the reactants. However, if the reactant molecules are strongly adsorbed but hardly react, the active sites will be poisoned. Moreover, fast desorption of the products reduces the chances of undesired secondary reactions and further increases the selectivity toward target products.[45−47]

To investigate the adsorption and desorption behaviors of the catalysts for isobutane and isobutene and their impacts on dehydrogenation performance, the transient response experiment as depicted in the Experimental Section was carried out on the apparatus displayed in Figure S1 in the Supporting Information. For both $13Ni/MgAl_2$ catalyst reacted for 0.5 h (when maximum cracking activity was achieved) and $13Ni/MgAl_2$−S catalyst reacted for 5 h (when maximum dehydrogenation activity was obtained), the transient response signals of Ar and isobutene during the adsorption processes at different temperatures are shown in Figure 6. It is apparent that the signal delay extent between isobutene and Ar of $13Ni/MgAl_2$ catalyst was much larger than that of $13Ni/MgAl_2$−S catalyst.

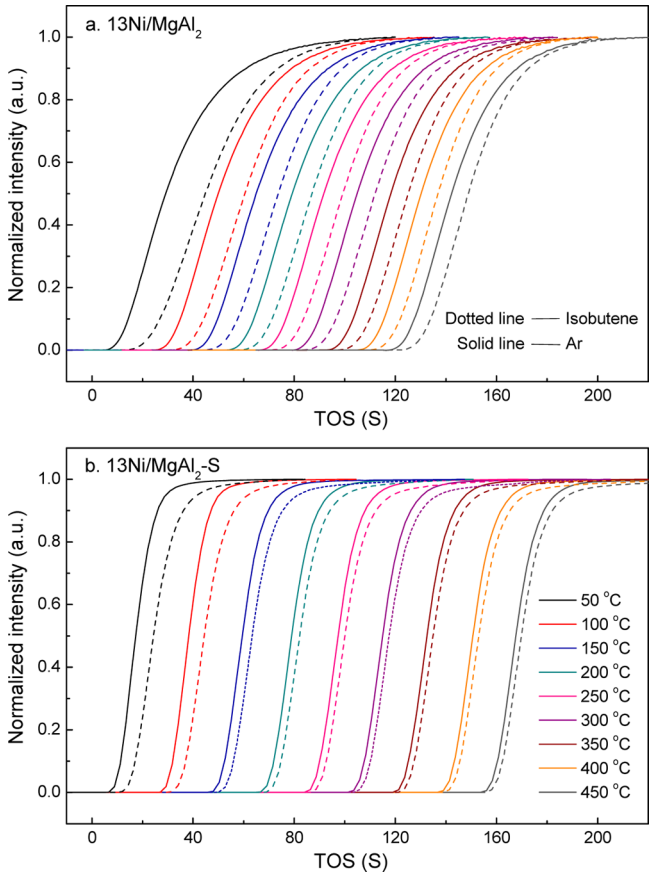

Figure 6. Transient response signals of Ar and isobutene over $13Ni/MgAl_2$ catalyst reacted for 0.5 h and $13Ni/MgAl_2$−S catalyst reacted for 5 h during the adsorption procedure.

dx.doi.org/10.1021/cs400705p | ACS Catal. 2013, 3, 2992−3001

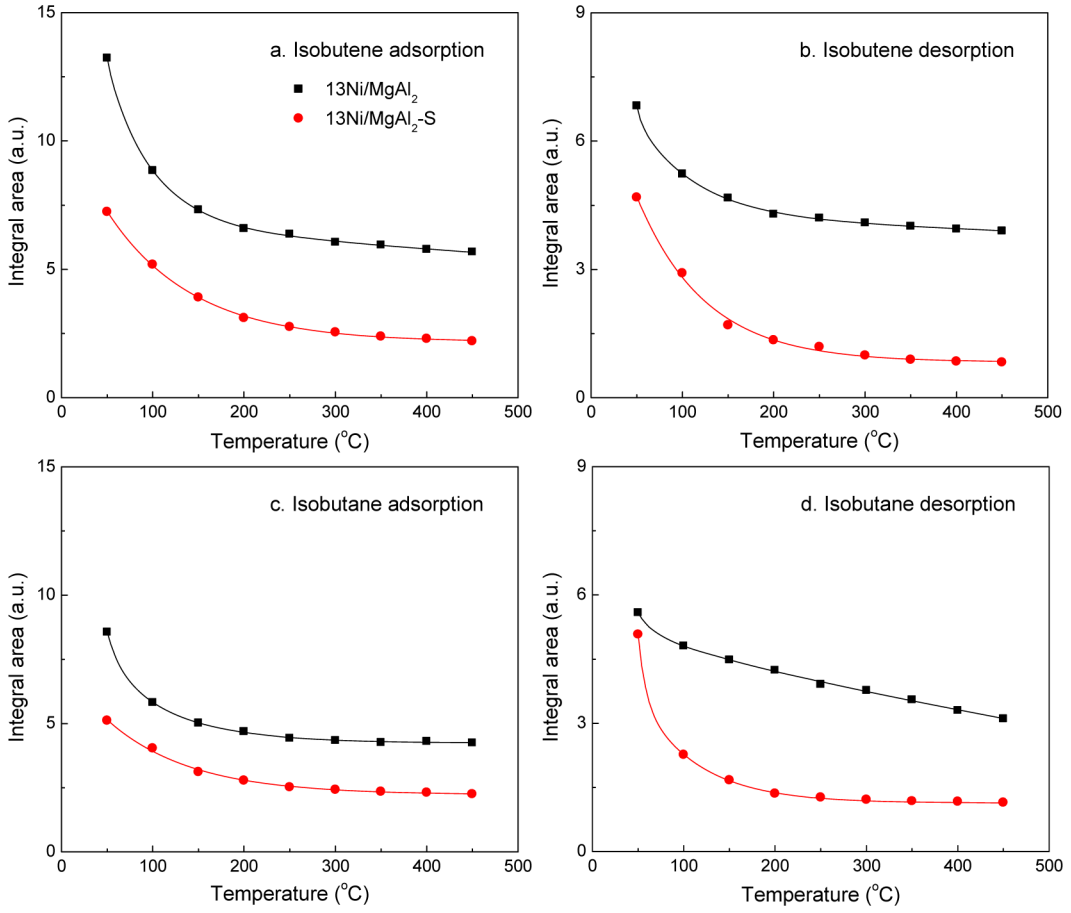

Figure 7. Integral area between Ar and hydrocarbon over 13Ni/$MgAl_2$ catalyst reacted for 0.5 h and 13Ni/$MgAl_2$−S catalyst reacted for 5 h during both adsorption and desorption procedures.

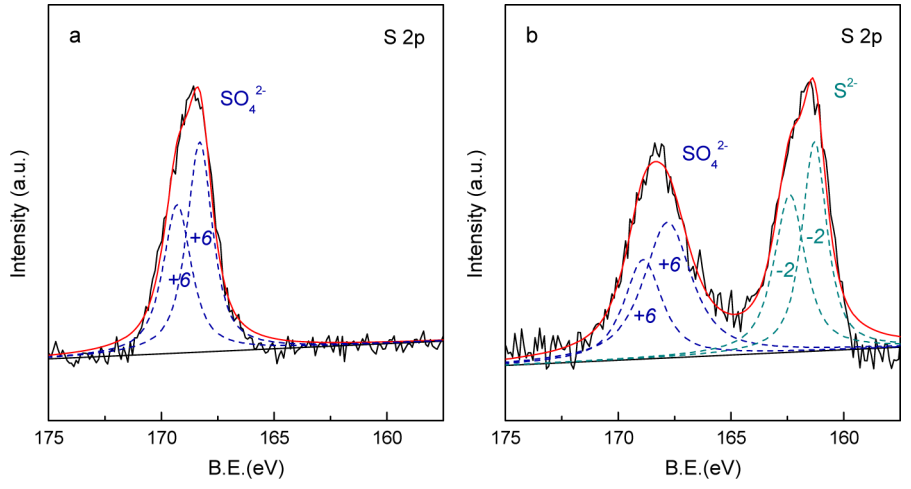

Figure 8. XPS spectra of 13Ni/$MgAl_2$−S catalysts before and after reaction: (a) fresh 13Ni/$MgAl_2$−S catalyst and (b) 13Ni/$MgAl_2$−S catalyst after 5 h reaction.

As described previously, a larger signal delay extent between hydrocarbon and inert gas in the adsorption process implies a stronger adsorption ability of the catalysts, while, that in the desorption process indicates more difficult desorption of the hydrocarbon instead. Therefore, compared with 13Ni/$MgAl_2$−S catalyst, the adsorption ability of 13Ni/$MgAl_2$ catalyst for isobutene is much stronger.

To clearly compare the distinction between the transient response signals, the area between the curves of Ar and isobutene was computed through integration of the difference, and the calculated adsorption areas are plotted as a function of temperature in Figure 7a. Similarly, the results of the desorption data for isobutene are also obtained and displayed in Figure 7b. Difficult desorption of alkenes from the nickel sites probably facilitates undesired secondary reactions and coke formation, and consequently, the active sites are covered by deposited coke and further deactivate. In this work, both smaller adsorption and desorption areas of isobutene were

dx.doi.org/10.1021/cs400705p | ACS Catal. 2013, 3, 2992−3001

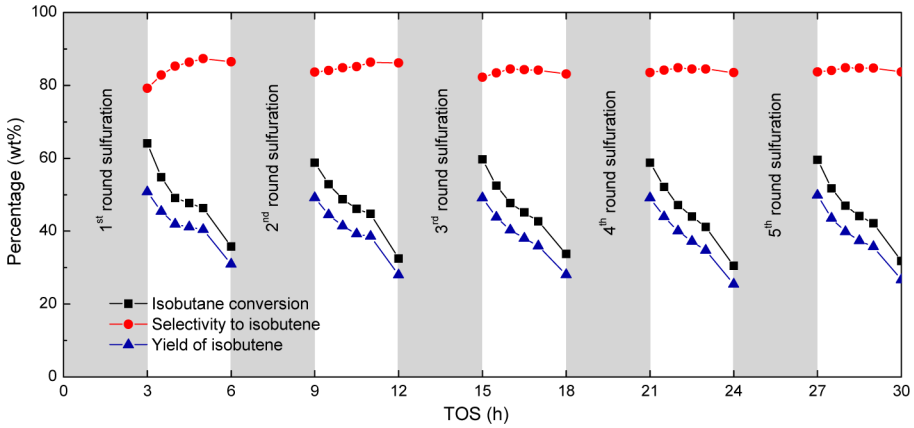

Figure 9. Catalytic performance of 13Ni/$MgAl_2$ catalyst (without sulfur addition) sulfurated by H_2S/H_2 for 3 h.

observed for 13Ni/$MgAl_2$−S catalyst, indicating much harder adsorption and easier desorption of the generated isobutene, and consequently, undesired secondary reactions were effectively inhibited and isobutene selectivity increased remarkably.

Furthermore, both larger integrated adsorption (Figure 7c) and desorption (Figure 7d) areas of isobutane were detected for the Ni/$MgAl_2$ catalyst, especially at higher temperatures. This result suggests that the catalyst before sulfur introduction possessed stronger adsorption ability of isobutane, but lower desorption ability, thus facilitating the conversion of isobutane.

3.3. Active Phase of Ni/$MgAl_2O_4$ Catalysts with Sulfur Addition. On the basis of the above discussions, the introduction of sulfur prevented the nickel oxide species from being aggregated, facilitated the desorption of isobutene generated, and thus reduced the possibility of occurrence of cracking reactions and undesired secondary reactions. However, the initial dehydrogenation activity of 13Ni/$MgAl_2$−S catalyst was relatively low, and an induction period was required to achieve the maximum activity. Observation of such an induction period suggested that the improved performance was probably related to the phase transformation of nickel species during the induction period, and the formation of a new active phase might be the real reason.

To investigate the variation of valence states of sulfur species during the induction period, XPS measurements were performed over both the fresh 13Ni/$MgAl_2$−S catalyst and the catalyst reacted for 5 h, when maximum catalytic activity was obtained. The S 2p XPS spectra are illustrated in Figure 8. For the fresh 13Ni/$MgAl_2$−S catalyst, only one oxidation state of sulfur with binding energy of S 2p between 168.5 and 169.5 eV, characteristic of sulfate species,[48,49] was detected. After the induction period, additional features with binding energy of S 2p around 161.7 eV, corresponding to the formation of S^{2-} species,[50,51] appeared. Therefore, it could be speculated that the nickel sulfide species formed during the reaction were probably the active phase for dehydrogenation, which contributed to the improved performance.

To verify the above speculation that NiS species constitute the active phase of ammonium sulfate modified catalysts for isobutane dehydrogenation, 13Ni/$MgAl_2$ catalyst was sulfurated by 10 vol.% H_2S/H_2 and further evaluated, which was similar with the sulfuration process in the hydrogenation reaction.[52,53] Figure S4 in the Supporting Information illustrates the dehydrogenation performance of 13Ni/$MgAl_2$ catalyst sulfurated by H_2S/H_2 at a reaction temperature of 560 °C for 1, 2, 3, and 5 h, respectively. For all the cases, the induction period disappeared, and the relatively high initial isobutane conversion indicates that the active phase NiS was probably formed during the sulfuration process. The initial isobutane conversion increased gradually with sulfuration time until 3 h, and after that the conversion decreased to some extent. Due to slight changes in isobutene selectivity arising from the different sulfuration processes used, isobutene yield exhibited a similar variation trend with that of isobutane conversion. To study the effect of sulfuration temperature (350, 450, 560, and 600 °C) on catalyst dehydrogenation performance, the sulfuration time was fixed at 3 h. As illustrated in Figure S5 in the Supporting Information, for the catalyst sulfurated at 350 °C, an obvious induction period could still be observed. With the increase of sulfuration temperature above 450 °C, the induction period disappeared, and the initial isobutane conversion first increased, and then decreased significantly. In consideration of isobutene yield, the optimum sulfuration temperature was about 560 °C, at which the highest initial isobutane conversion and isobutene yield were both obtained. In conclusion, the catalyst sulfurated at 560 °C for 3 h exhibited the best dehydrogenation performance (as shown in Figure 9), for which the initial isobutane conversion up to ∼64 wt % and relatively high selectivity to isobutene were obtained.

The sulfurated 13Ni/$MgAl_2$ catalyst under the optimum sulfuration conditions was also characterized by XRD and the patterns are illustrated in Figure 2. In addition to diffraction peaks of fresh 13Ni/$MgAl_2$ catalyst, additional characteristic peaks of NiS at 30.1°, 34.7°, and 53.5° were also detected, in accordance with the results of XPS characterization obtained for 13Ni/$MgAl_2$−S catalyst. Therefore, the conclusion can be drawn that, for the Ni/$MgAl_2O_4$ catalyst with sulfur addition, NiS species, formed during both the reaction and sulfuration processes, are the real active phase for isobutane dehydrogenation.

Furthermore, possibly because of the consumption of the active phase, the catalyst activity decreased gradually with TOS. For the sulfurated catalyst reacted for 3 h, characterization peaks of Ni_7S_6 were observed in the XRD patterns (see Figure 2), suggesting that sulfur loss was the real reason for catalyst deactivation during the reaction. An online MS was applied to detect the gas released during isobutane dehydrogenation over the sulfurated catalyst. In the MS spectra (as illustrated in Figure S6 in the Supporting Information), H_2S (m/z = 34) was detected and its intensity decreased gradually with time on

dx.doi.org/10.1021/cs400705p | ACS Catal. 2013, 3, 2992−3001

stream, suggesting that the sulfur was lost mainly in the form of H_2S.

To recover the activity, the catalyst was sulfurated by H_2S/H_2 for another 3 h after every 3 h reaction, and totally five such sulfuration-reaction cycles were carried out. As displayed in Figure 9, for each cycle, the catalyst activity could be completely restored by the sulfuration treatment, further confirming that the existence of sulfur is essential for achieving excellent dehydrogenation performance.

4. CONCLUSIONS

$Ni/MgAl_2O_4$ catalysts with different NiO loading amounts exhibited different performances in isobutane dehydrogenation. Catalysts with low NiO content possessed low catalytic activity. Although the activity was improved at higher NiO loadings, because of the formation of aggregated metallic nickel species during the initial reduction period, which was verified by XRD characterization, undesirable cracking reactions were intensified and isobutene selectivity was worsened.

To improve the catalytic performance, sulfur was introduced into the $Ni/MgAl_2O_4$ catalysts. Characterization results obtained in SEM and adsorption−desorption tests for isobutane and isobutene indicated that NiO particles were well dispersed and isobutene desorption was facilitated after sulfur introduction. Consequently, cracking reactions were effectively inhibited, and the selectivity to isobutene increased remarkably. Furthermore, an XPS study together with an activity test jointly revealed that, for $Ni/MgAl_2O_4$ catalyst with sulfur addition, NiS was the real active phase for isobutane dehydrogenation.

Through sulfuration with H_2S/H_2, a high initial activity was achieved for $Ni/MgAl_2O_4$ catalyst. Subsequently, with the consumption of sulfur species, the isobutane conversion decreased gradually with TOS. After sulfuration treatment with H_2S/H_2 again, the catalyst activity could be completely recovered, fully demonstrating the crucial role that the introduced sulfur played.

■ ASSOCIATED CONTENT

Supporting Information

Further details are given in Figures S1−S6. This material is available free of charge via the Internet at http://pubs.acs.org.

■ AUTHOR INFORMATION

Corresponding Author

*E-mail: chyli@upc.edu.cn, chyli_upc@126.com.

Notes

The authors declare no competing financial interest.

■ ACKNOWLEDGMENTS

This work was financially supported by the National Natural Science Foundation of China (No. U1362201), the National 973 Program of China (No. 2012CB215006), and the Fundamental Research Funds for the Central Universities (No. 12CX06040A).

■ REFERENCES

(1) Zimmermann, H.; Versluis, F. U.S. Patent 5378350, 1995.
(2) Buonomo, F.; Jezzi, R.; Notari, B.; Kotelnikov, G. R.; Michailov, K. R.; Patanov, V. A. U.S. Patent 4746643, 1988.
(3) Fritz, P. M.; Boelt, H. V.; Hackner, H.; Van, D. G. J. EP Patent 0947247, 1999.
(4) Iezzi, R.; Buonomo, F.; Sanfilippo, D. U.S. Patent 5143886, 1992.
(5) Herber, R. R.; Thompson, G. J. U.S. Patent 4806624, 1989.
(6) Olbrich, M. E.; McKay, D. L.; Montgomery, D. P.; Jean, B. U.S. Patent 4926005, 1990.
(7) Lin, J. H.; Biswas, P.; Guliants, V. V.; Misture, S. *Appl. Catal. A: Gen.* **2010**, *387*, 87−94.
(8) Xu, J.; Froment, G. F. *Aiche J.* **1989**, *35*, 88−96.
(9) Li, Y.; Fu, Q.; Flytzani-Stephanopoulos, M. *Appl. Catal. B: Environ.* **2000**, *27*, 179−191.
(10) Zeppieri, M.; Villa, P.; Verdone, N.; Scarsella, M.; De Filippis, P. *Appl. Catal. A: Gen.* **2010**, *387*, 147−154.
(11) Rostrup-Nielsen, J. R. *J. Catal.* **1984**, *85*, 31−43.
(12) Cerritos, C. R.; Ramirez, F. R.; Alvarado, A. A. F.; Rosales, M. n. J.M.; Garcia, V. T; Esquivel, G. I. R. *Ind. Eng. Chem. Res.* **2010**, *50*, 2576−2584.
(13) Fatsikostas, A. N.; Verykios, X. E. *J. Catal.* **2004**, *225*, 439−452.
(14) Georgiadis, R.; Fisher, E. R.; Armentrout, P. *J. Am. Chem. Soc.* **1989**, *111*, 4251−4262.
(15) Freas, R. B.; Campana, J. E. *J. Am. Chem. Soc.* **1986**, *108*, 4659−4661.
(16) Halle, L.; Houriet, R.; Kappes, M. M.; Staley, R. H.; Beauchamp, J. *J. Am. Chem. Soc.* **1982**, *104*, 6293−6297.
(17) Byrd, G.; Burnier, R.; Freiser, B. *J. Am. Chem. Soc.* **1982**, *104*, 3565−3569.
(18) Van Koppen, P. A.; Brodbelt-Lustig, J.; Bowers, M. T.; Dearden, D. V.; Beauchamp, J.; Fisher, E. R.; Armentrout, P. *J. Am. Chem. Soc.* **1990**, *112*, 5663−5665.
(19) van Koppen, P. A.; Bowers, M. T.; Haynes, C. L.; Armentrout, P. *J. Am. Chem. Soc.* **1998**, *120*, 5704−5712.
(20) Jacobson, D.; Freiser, B. *J. Am. Chem. Soc.* **1983**, *105*, 5197−5206.
(21) Resasco, D. E.; Marcus, B. K.; Huang, C. S.; Durante, V. A. *J. Catal.* **1994**, *146*, 40−55.
(22) Labinger, J. A.; Bercaw, J. E. *Nature* **2002**, *417*, 507−514.
(23) Fokin, A. A.; Schreiner, P. R. *Chem. Rev.* **2002**, *102*, 1551−1594.
(24) Nakagawa, K.; Kajita, C.; Okumura, K.; Ikenaga, N.; Nishitani Gamo, M.; Ando, T.; Kobayashi, T.; Suzuki, T. *J. Catal.* **2001**, *203*, 87−93.
(25) Watson, R. B.; Ozkan, U. S. *J. Catal.* **2000**, *191*, 12−29.
(26) Carrera Cerritos, R. l.; Fuentes Ramirez, R.; Aguilera Alvarado, A. F.; Martinez Rosales, J. M.; Viveros Garcia, T. s.; Galindo Esquivel, I. R. *Ind. Eng. Chem. Res.* **2010**, *50*, 2576−2584.
(27) Parmaliana, A.; Arena, F.; Frusteri, F.; Giordano, N. *J. Chem. Soc., Faraday Trans.* **1990**, *86*, 2663−2669.
(28) Mondal, D.; Villemure, G.; Li, G.; Song, C.; Zhang, J.; Hui, R.; Chen, J.; Fairbridge, C. *Appl. Catal. A: Gen.* **2013**, *450*, 230−236.
(29) Duchet, J. C.; van Oers, E. M.; de Beer, V. H. J.; Prins, R. *J. Catal.* **1983**, *80*, 386−402.
(30) Louwers, S. P. A.; Prins, R. *J. Catal.* **1992**, *133*, 94−111.
(31) Haber, J.; Lalik, E. *Catal. Today* **1997**, *33*, 119−137.
(32) Chen, M.; Wu, J. L.; Liu, Y. M.; Cao, Y.; Guo, L.; He, H. Y.; Fan, K. N. *Appl. Catal. A: Gen.* **2011**, *407*, 20−28.
(33) Chen, M.; Xu, J.; Liu, Y. M.; Cao, Y.; He, H. Y.; Zhuang, J. H. *Appl. Catal. A: Gen.* **2010**, *377*, 35−41.
(34) Chen, M.; Xu, J.; Cao, Y.; He, H. Y.; Fan, K. N.; Zhuang, J. H. *J. Catal.* **2010**, *272*, 101−108.
(35) Gascón, J.; Téllez, C.; Herguido, J.; Menéndez, M. *Appl. Catal. A: Gen.* **2003**, *248*, 105−116.
(36) Cortright, R. D.; Hill, J. M.; Dumesic, J. A. *Catal. Today* **2000**, *55*, 213−223.
(37) Airaksinen, S. M.; Harlin, M. E.; Krause, A. O. I. *Ind. Eng. Chem. Res.* **2002**, *41*, 5619−5626.
(38) Cortright, R. D.; Levin, P. E.; Dumesic, J. A. *Ind. Eng. Chem. Res.* **1998**, *37*, 1717−1723.
(39) Coughlin, R. W.; Hasan, A.; Kawakami, K. *J. Catal.* **1984**, *88*, 163−176.
(40) Coughlin, R. W.; Kawakami, K.; Hasan, A. *J. Catal.* **1984**, *88*, 150−162.
(41) Biloen, P.; Helle, J. N.; Verbeek, H.; Dautzenberg, F. M.; Sachtler, W. M. H. *J. Catal.* **1980**, *63*, 112−118.

(42) Mosayebi, Z.; Rezaei, M.; Ravandi, A. B.; Hadian, N. *Int. J. Hydrogen Energy* **2012**, *37*, 1236−1242.
(43) Park, D. S.; Li, Z.; Devianto, H.; Lee, H.-I. *Int. J. Hydrogen Energy* **2010**, *35*, 5673−5680.
(44) Guo, J.; Lou, H.; Zhao, H.; Chai, D.; Zheng, X. *Appl. Catal. A: Gen.* **2004**, *273*, 75−82.
(45) Gründling, C.; Eder-Mirth, G.; Lercher, J. A. *J. Catal.* **1996**, *160*, 299−308.
(46) Chen, Y.; Guo, Z.; Chen, T.; Yang, Y. *J. Catal.* **2010**, *275*, 11−24.
(47) Mallat, T.; Baiker, A. *Chem. Rev.* **2004**, *104*, 3037−3058.
(48) Yu, X.; Liu, F.; Wang, Z.; Chen, Y. *J. Electron Spectrosc.* **1990**, *50*, 159−166.
(49) Portela, L.; Grange, P.; Delmon, B. *J. Catal.* **1995**, *156*, 243−254.
(50) Laurenti, D.; Phung-Ngoc, B.; Roukoss, C.; Devers, E.; Marchand, K.; Massin, L.; Lemaitre, L.; Legens, C.; Quoineaud, A. A.; Vrinat, M. *J. Catal.* **2013**, *297*, 165−175.
(51) Polyakov, M.; van den Berg, M. W. E.; Hanft, T.; Poisot, M.; Bensch, W.; Muhler, M.; Grünert, W. *J. Catal.* **2008**, *256*, 126−136.
(52) Okamoto, Y.; Hioka, K.; Arakawa, K.; Fujikawa, T.; Ebihara, T.; Kubota, T. *J. Catal.* **2009**, *268*, 49−59.
(53) Okamoto, Y.; Kato, A.; Usman; Rinaldi, N.; Fujikawa, T.; Koshika, H.; Hiromitsu, I.; Kubota, T. *J. Catal.* **2009**, *265*, 216−228.